Paddy Rice Monitoring Using TanDEM-X

Cristian Rossi and Esra Erten, *Member, IEEE*

***Abstract*—This paper evaluates the potential of spaceborne bistatic interferometric SAR images for the monitoring of biophysical variables in wetlands, with a special interest on paddy rice. The assessment is made during the rice cultivation period, from transplanting to harvesting time (May to October) for fields around Gala lake (Turkey), one of the largest and most productive paddy rice planting area in the country. Detailed ground truth measurements describing biophysical parameters are collected in a dedicated campaign. A stack of 16 dual-pol TanDEM-X images is used for the generation of 32 Digital Elevation Models (DEMs) over the studied area. The quality of the data allows the use of the interferometric phase as a state variable capable to estimate crop heights for almost all the growing stages. The early vegetative rice stage, characterized by flooded fields, cannot be represented by the interferometric phase due to a low Signal-to-Noise-Ratio (SNR) but can be easily detected by amplitude and interferometric coherence thresholding. A study on the impact of the polarization in the signal backscatter is also performed. An analysis of the differences between HH and VV DEMs shows the varying signal penetration for the two polarizations at different growing stages. The validation with reference data demonstrates the capability to establish a direct relationship between interferometric phase and rice growth. The very high coherence of TanDEM-X data yields elevation estimates with root mean square error in a decimetric level, supporting temporal change analysis on a field-by-field basis.**

***Index Terms*—TanDEM-X, agriculture, paddy-rice monitoring, synthetic aperture radar interferometry, polarimetry, DEM**

I. Introduction

Remote sensing is a mature technology for observation of natural environmental changes. In terms of agricultural monitoring applications, radar sensors differ from optical, multispectral and thermal sensors. First, radar imaging provides a timely mapping of the scattering properties of biophysical variables, including night and all weather condition monitoring. Second, the system not only measures amplitudes but also phases of the backscattered signal, yielding the joint derivation of absolute ranging and backscattering coefficients. Hence, for crop inspection applications, temporal Synthetic Aperture Radar (SAR) images are an attractive instrument to exploit.

For more than 10.000 years, rice has been one of the most important products in food market. Rice agriculture, which is considered a seasonal planting, is mainly possible in temperate climates. A rice growth cycle from panicle initiation to maturing, takes about 110-250 days. Throughout this cycle, roots and bottom part of the stem stay submerged in water for approximately 90 days. The rice growth cycle mainly consists of three stages: *vegetative*, *reproductive* and *maturation*. In these phenological stages, rice plants exhibit distinct structural differences. These differences are described by using a scale called *Biologische Bundesanstalt, bundessortenamt und CHemische industrie* (BBCH) [1]. All growing stages can be associated with the BBCH-scale, as shown in Table I. In response to the increasing demand of rice, monitoring of farming activities cannot be left only to farmers. Information on crop activities is also significant to governments for planning strategies. Specifically, observations with remote sensing technologies are urgent for developing countries. In this case, considering that rice fields are generally cultivated under cloudy and rainy weather, radar remote sensing is of particular interest in their monitoring.

Accordingly, SAR images have been already used for several campaigns for crop inspections [2]–[10]. [2] made an analysis to determine the most suitable combination of frequency, polarization and incidence angle for rice monitoring. The main outcome of the study is the definition of a relationship between the C-band backscatter coefficient and the *Leaf Area Index* (LAI), provided also by [11]. Following this work and exploiting the RADARSAT mission, several other researches on C-band rice monitoring are reported [3], [9]. These researches underline how temporal C-band backscatter depends on the biophysical stage of the crop. However, due to the limited information about biophysical parameters obtained from single channel SAR images, it is not easy to calculate some physical parameters as *height above ground*, *number of leafs*, and *leaf angle* directly from backscattering coefficients. [12]–[16] underlined the potential of multiple polarimetric measurements in rice monitoring. These studies, employing a time series analysis, reported the relationship between BBCH-scale and polarimetric observables as *entropy*, *alpha*, ratio and coherence between HH and VV polarized images.

Many possible measures of rice growth as canopy height, LAI, biomass, etc. are considered in the works cited above. Among them, canopy height is the most direct measurement and has direct relationship with growth rate, especially in the vegetative stage. [2], [10] reported the correlation between canopy height and backscattering coefficients, although the scattering process is not a function depending only on crop height. In fact, an indirect relationship can be assessed. As the canopy gets higher, a double-bounce scattering mechanism generated by the interaction between the stems and the underlying water surface yields high reflections. This relationship is reported to vary among frequency bands [4], [17]. These works analyze the electromagnetic scattering which is a function of intricate interrelations among physical parameters of rice. Moreover, as based on experimental data sets and locally selected thresholds, their accuracy may be insufficient for operational processors commanded to process various data sets.

C. Rossi is with Remote Sensing Technology Institute, German Aerospace Center (DLR), $D-82234$ Oberpfaffenhofen, Germany (e-mail:cristian.rossi@dlr.de).

E. Erten is with the department of Geomatics Engineering, Istanbul Technical University (ITU), $TR-34469$ Istanbul, Turkey (e-mail:eerten@itu.edu.tr).

Next to single-image back-scattering information, interferometric phase information provides an additional support with the cost of two SAR images. From an agricultural application point of view, in the literature, interferometric phase information has been employed by exploiting the coherence as in [18]–[20]. In these works, most of the attention has been given on the accuracy of the interferometric phase in tandem data set. However, ERS data set with low resolution can not tackle the physical-based spatial heterogeneity problem in paddy rice fields. The use of *differential* interferometric phase, which is a direct function of temporal volume change, is also rare in paddy rice monitoring literature. Instead, several studies have been reported for soil moisture modeling [21], glacier [22], seismic events [23] and urban area [24] volume changes. These previous volume studies emphasize that two aspects have to be considered in terms of monitoring applications. The first one is the potential penetration, causing an underestimation in volume deviations. The second one is the large temporal baselines, causing unreliable interferometric phase information. A promising SAR mission to attenuate these limitations is TanDEM-X [25], which allows to measure small phase center variations related to the changes in canopy height, since the relatively short X-band wavelength interacts mostly with upper sections of the crop. The objective of this work is to examine the relationship between crop height and differential interferometric phase for paddy rice and to explore the new capabilities of TanDEM-X monitoring for assessment of crop growth. TanDEM-X is an innovative SAR concept, first in space making use of a bistatic configuration to generate high-resolution Digital Elevation Model (DEM) accomplishing HRTI-3 accuracy requirements. The flexible commanding yields the acquisition of several DEMs over the same area in a short revisit time. In this paper, a stack of 16 dual-pol acquisitions over one of the largest and most productive paddy rice planting area in Turkey, around Gala lake, is analyzed. The differential interferometric phase is derived and used as a *state* variable to describe the rice phenological stage. The limitations depicted above, i.e. the difficulties to relate a backscatter analysis with a derivation of crops height and the difficulties to establish operational schemes, are reduced by employing the bistatic system.

Major Stage	BBCH Scale	Description
Vegetative	00	Germination
	10	Leafing
	20	Tillering
	30	Stem elongation
	40	Booting
Reproductive	50	Heading
	60	Flowering
	70	Fruiting
Maturation	80	Ripening
	90	Senescence

TABLE I
BBCH SCALE OF RICE

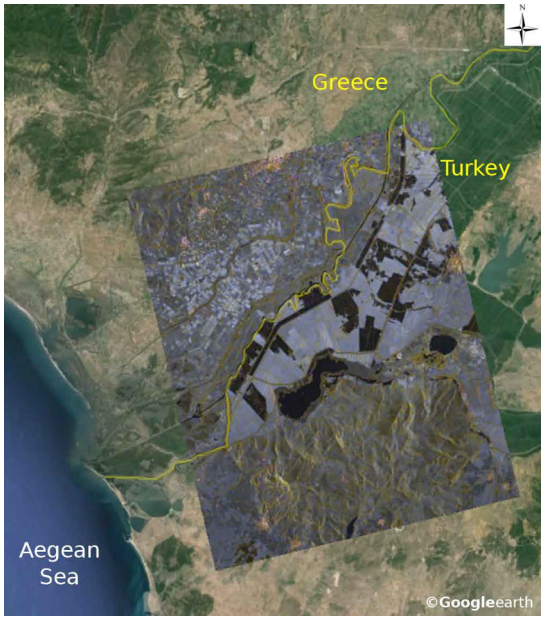

Fig. 1. RGB composite master amplitude acquired on the 12.05.2012 showing the location of the study area.

TanDEM-X data has been recently analyzed in [26] with outcomes strongly limited by the small baselines of the experimental acquisitions. Moreover, low SNR was an issue by producing low coherence in the growing stages. For the case under study, the TanDEM-X experimental dataset has baselines well suitable for an interferometric analysis. To present the first TanDEM-X results with the aim of crop height monitoring, this paper is organized as follows. In Section II, the test site and the ground measurement campaign are described, leading to the problem formulation of temporal growth change. Next section is dedicated to the processing strategies employed for the derivation of change maps using the data stack. The extraction of crop heights without using external data is also outlined in here. The validation and establishment of a relationship between rice phenology and interferometric height is then presented. Section IV concludes this paper revisiting and synthesizing the above considerations.

II. Test Site and Ground Measurement Campaign

The lower course of the Maritsa river and surrounding, where it forms the border of Greece and Turkey, is a unique wetland environment consisting of lakes, rivers and agricultural fields (see Fig.1). In the last 50 years, changes in topography due to debris flow and heavy rain affecting the regional ecosystem were measured. Recently, the region is controlled by the government and made available for agricultural practice, mainly for paddy rice. Considering the regional risk of debris flow, agricultural fields have to be monitored, controlling by this way the effect of flow. For instance, if the seeding has been affected from flow and irrigation, farmers can do transplanting again before it is too late for seeding.

In order to better understand the microwave interaction with agricultural fields, the state organization Trakya Agricultural Research Institute collected detailed ground truth in 8 fields

Fig. 2. The first line shows portions of agricultural fields acquired on the 30^{th} of May, 2013, illustrating the differences in agricultural practice. The second line shows the temporal pictures of field 8.

with 4 independent samples per field during the growth cycle (May to October) of paddy rice in 2013. *Height above ground and water*, *number of plants per area*, *number of leaves per area*, *number of tillers per area*, *number of panicles per area*, *stem diameter*, *leaf width*, *leaf length* and *leaf angle* were collected in the fieldwork. The fieldworks dates are illustrated in Fig. 2 with the pictures taken during these studies. To highlight the spatial variation in response to changes in agricultural practice, the first line in Fig. 2 shows the pictures taken from different fields on the same day. In this region different fields are cultivated variously depending on the field owner decision. Despite their variety in cultivating, the phenological evolution (BBCH-scale) of the monitored parcels is similar but shifted in time (see Fig. 3(a)). Since their temporal trends are similar, in the second line of Fig. 2, temporal pictures simultaneously taken in the fieldworks are shown only for a single field (field 8). In the study area, the sowing method is direct seeding by broadcasting, implying a random seeding instead of a regular straight-row one.

The phenological development of these fields shows a clear similar trend with the rice field monitored in Sevilla, Spain by [17]. However, it is important to underline that the differential slope indicating the step from reproductive stage to maturation stage is higher in the Sevilla campaign then in the Gala Lake one. In [17], a classification of BBCH-scales is done based on a set of rules obtained from the Sevilla dataset. Using the same decision tree may bring inaccuracies in other study areas.

Considering the interest in volume changes of agricultural fields, Fig. 3 shows the plots of the relationship between canopy height, BBCH-scale and day of the year obtained during the field works. Most fields were homogeneous and crops reached maximum height after flowering. As Fig. 2 illustrates, when crop reaches the flowering stage it is fully developed with no gaps between plants. During the cultivation period, the monotonous relationship between canopy height and BBCH-scale in Fig. 3(b) makes the elevation monitoring appealing. To be noticed, height sensitivity to crop development is particularly high up to about BBCH 60. After this stage, plant height exhibits just small changes. In Section I it is outlined how backscattering coefficients of radar signal do not allow a direct detection of BBCH-stages due to lack of detectable physical changes in the phenology. Thus, in this paper, the earlier analysis based on backscattering coefficients is extended, and the differential interferometric phase is explored in terms of biophysical parameters in the next section.

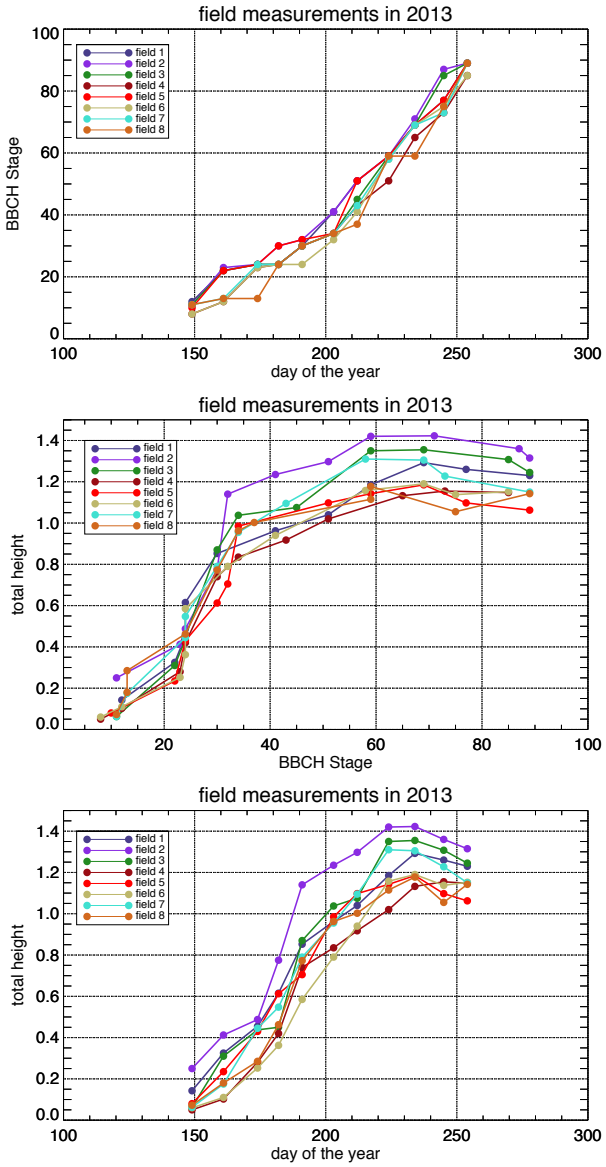

Fig. 3. The biophysical stage characterized by BBCH scale of the monitored 8 fields as a function of day of year (a) and of height above the ground (b). The relationship between the day of the year and the canopy total height (c).

III. Processing results and validation

In the framework of the German Aerospace Center (DLR) project $XTILAND1476$, 16 dual-pol TanDEM-X acquisitions have been acquired over the Gala lake region in 2012 and 2013. Specifically, 9 acquisitions have been commanded in 2012 and 8 in 2013 at the same incidence angle. As shown in Tab. II, only the 2012 acquisitions are covering all the rice growing stages (May to October), whereas the 2013 acquisitions are missing the maturation stage (August to October). For this reason, even though the GPS campaign has been conducted in 2013, the sole 2012 acquisitions are employed in the following analysis. An additional reason relies to the height sensitivity of the different bistatic configurations. Height of Ambiguity (HoA), an important system parameter describing the elevation range of a phase cycle - smaller it is more accurate the generated DEM -, is ranging between about 20 and 30 meters for the 2012 acquisitions and between about 40 and 50 meters for the 2013 ones. To give a quantitative idea, assuming a Gaussian distributed phase error, a coherence value of 0.8 yields a standard error of 0.36 meters for the 12.05.2012 processed configuration (HoA: 23.1 m) and a standard error of 0.84 meters for the 26.07.2013 one (HoA: 52.8 m) [27].

The data stack is processed with the Integrated TanDEM-X Processor (ITP) at the DLR processing facilities [28]. ITP is the operational system employed in the TanDEM-X mission for the generation of the raw DEM given as input SAR raw data. The processor is commanded to generate HH and VV DEMs, for a total of 32 DEMs, with an output raster of 6 meters. As in Table II, the interferogram resolution is triggered to be around 10 meters by multi-looking the input co-registered data, yielding height errors at a coherence value of 0.8 specified in the last column of the table. Considering the purpose of tracking crop height in all the growing stages, multi-looking process is a necessary step to reduce the phase noise and the resulting standard error to a decimetric level. Due to the relatively smooth topography of the scenes, phase unwrapping is not an issue (even for small height of ambiguities) and no unwrapping errors have been detected. To ensure a straightforward analysis, all the DEMs have been generated at the same output grid and have been equally calibrated jointly using SRTM and ICESat data. For the following analysis, the HH channel has been chosen. Nevertheless, a study with the differences observed between the different polarizations is provided in the following section.

A. Dual-polarization study

Before studying the differential interferometric phase with the crop height estimation purpose, the temporal trend of backscattering coefficients represented by σ^0 is examined. The image intensity values for HH and VV polarizations are transformed to σ^0 according to [29] and plotted in Fig 4(a). The different agricultural practices can be seen by comparing the various fields on the time line. As reported in [6], HH/VV ratio is an excellent indicator of rice phenological stages, thus, it is also plotted in Fig. 4(b). As expected, the temporal trend of the backscattering information is similar to the previous detailed work at X-band in [17]. HH/VV ratio is sensitive to rice phenology due to both the attenuation depending on the incidence wave polarization and the dominance of the double-bounce interaction between stems and flooded ground.

An investigation of polarization-dependent penetration depths is meaningful for crop height monitoring. Over automatically selected fields (see next section), HH and VV polarized interferograms are transformed to surface height values. Their relationship, demonstrated by scatter plots of the observed HH and VV height values, is temporarily analyzed

TABLE II
MAIN PARAMETERS OF THE INTERFEROMETRIC DATA SET (HH CHANNEL)

acquisition date (DOY)		center incidence angle [deg]	perpendicular baseline [m]	height of ambiguity [m]	interferogram resolution [m]	standard error* [m]
12.05.2012	(133)	36.8	253.7	23.1	10.2	0.36
14.06.2012	(166)	36.8	242.3	24.2	10.3	0.38
06.07.2012	(188)	36.8	234.3	25.1	10.2	0.40
17.07.2012	(199)	36.8	227.2	25.8	10.2	0.41
28.07.2012	(210)	36.8	222.7	26.3	10.3	0.42
19.08.2012	(232)	36.8	213.4	27.4	10.2	0.43
10.09.2012	(254)	36.8	204.4	28.7	10.3	0.46
13.10.2012	(297)	36.8	187.1	31.3	10.3	0.50
26.11.2012	(331)	36.8	181.3	32.3	10.3	0.51
05.03.2013	(64)	36.8	112.0	52.8	10.4	0.83
16.03.2013	(75)	36.8	111.5	53.1	10.4	0.84
10.05.2013	(130)	36.8	139.7	42.1	10.4	0.67
21.05.2013	(141)	36.8	141.1	41.6	10.3	0.66
01.06.2013	(152)	36.8	146.6	40.2	10.3	0.63
23.06.2013	(174)	36.8	144.3	40.7	10.4	0.64
26.07.2013	(207)	36.8	111.6	52.8	10.3	0.84

*Standard error computed at a coherence value of 0.8 for an equivalent number of looks of about 30.

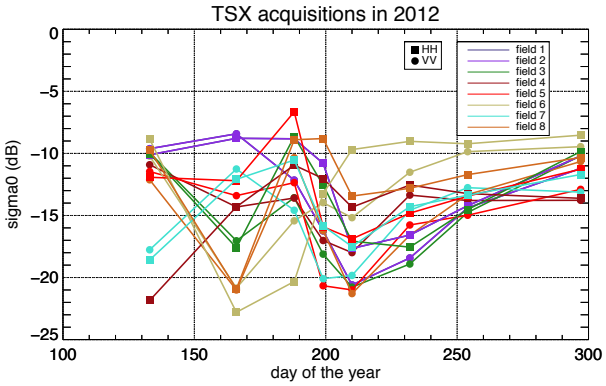

(a)

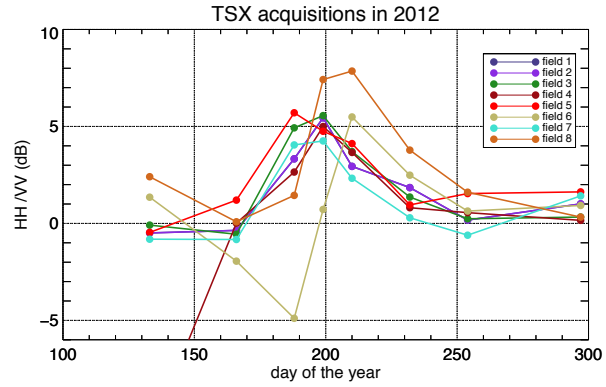

(b)

Fig. 4. (a) Measured backscattering coefficients in HH and VV polarization. (b) Polarimetric ratio $\sigma^0_{HH}/\sigma^0_{VV}$.

as shown in Fig. 5. The temporal scatter plots exhibit a strong linear relationship between the observations. Nevertheless, slight elevation differences are measured depending on the phenological stage of the crop. Although the scatter plots in Fig. 5(a) and Fig. 5(d) show very little height discrepancies for different polarizations, the ones in Fig. 5(b) and Fig. 5(c) have higher differences. The BBCH-scale of the crop is 78 and 95 on August 19 and September 10, respectively, indicating that the crop was extremely dry (see also Fig. 2). With such a dry vegetation layer, the X-band radar signal penetrates into the canopy with different penetration length depending on the polarization. This difference is related to the fact that HH signal penetrates more effectively into canopies than the VV does [30]. It can be noticed that rice canopy is mainly vertically oriented until the beginning of August, then the orientation becomes random after flowering stages (fruiting, ripening and senescence), meaning that the effects of canopy orientation on the penetration depth can be ignored. Considering quantitative analysis, the correlation between the height measurements obtained from HH and VV polarized images is examined using linear regression. High temporal correlation values such as $R = \{0.982, 0.984, 0.981, 0.987\}$ are almost the same and not changeable depending on the phenological stage of the canopy. However, the disturbance term, which is related to the differences between HH and VV observations, is changing depending on the phenological stage.

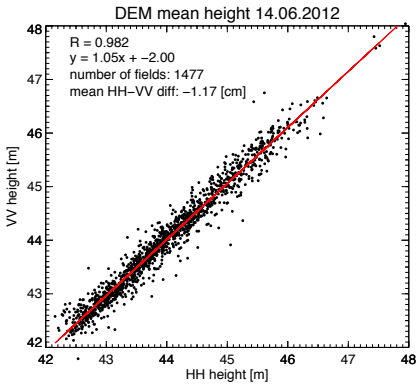

(a)

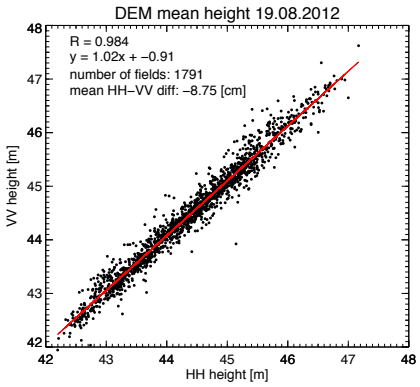

(b)

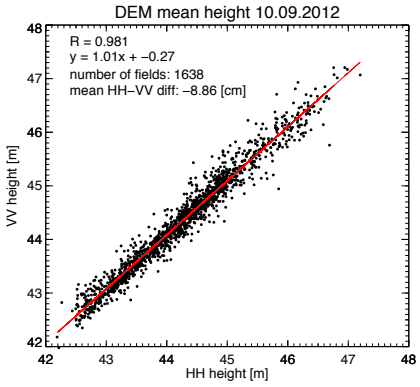

(c)

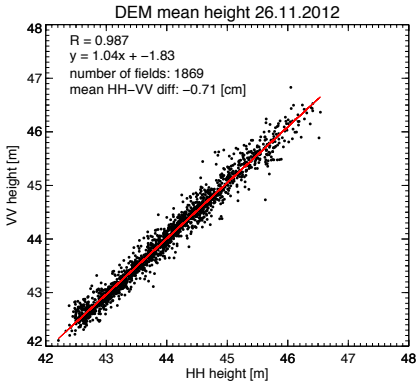

(d)

Fig. 5. The height measurements obtained by HH and VV polarized images over the selected agricultural fields for four different dates.

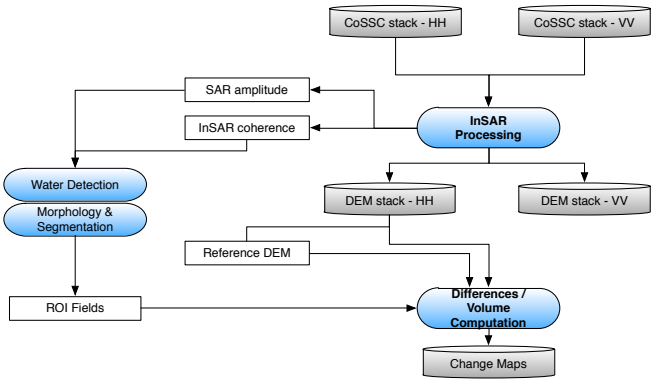

Fig. 6. Flowchart with the processing strategy employed for the analysis.

The height differences obtained from HH and VV polarized interferograms increase about 8 cm in maturation stages as expected from the above considerations. Additionally, over the detected agricultural fields the average coherence for HH and VV polarized interferograms acquired on August 19 and on September 10 are analyzed. A standard deviation of 0.06 and 0.03 is obtained for VV and HH polarized interferometric coherences, respectively. This also proofs that HH polarized signal has the ability to penetrate more stable into the canopy when it is dry as the interior part of the rice plant provides a more stable return than the surface component.

B. Interferometric phase study

A strategy to evaluate the potential of the differential interferometric SAR data is assessed in this section and outlined in Fig. 6. The input coregistered complex data stack (CoSSC stack) is processed in ITP for both polarimetric channels. ITP is specially triggered to output an equally calibrated DEM stack by using external information. In particular, a SRTM DEM calibrated with ICESat is used in the absolute phase offset stage for all the DEMs in order to provide consistent outputs without discrepancies among them [28]. As seen in Section III-A, the two polarization channels yield the generation of very similar elevation profiles - ignoring the early vegetative stage -, with centimeter inconsistencies in the maturation stage (dry season). Thus, just a single channel, HH, is chosen for the analysis.

The main scope of the interferometric investigation is the verification of rice stages by using temporal elevation data. To this aim, field segmentation is mandatory, reasonably assuming a consistent growing within single fields. An important sub-product to exploit, generated during the interferometric processing, is the coherence. By describing the similarity of the coregistered complex master and slave data, the coherence is a considerable input for the analysis, supporting the segmentation algorithm. As described in Section II, flooded parcels of land characterize the early vegetative state. During this state, fields are covered by water and separated by a path network composed by soil or rare grass, as visible also in Fig. 8, representing the May 2012 acquisition. A gravel road network is also in the test site separating parcel groups. This natural segmentation is well visible by inspecting the interferometric coherence in Fig. 8(b), as good as inspecting the master channel amplitude in Fig. 8(a). This visibility relies on the water body electromagnetic spectrum. Non-moving water behaves like a mirror, reflecting the incident signal wave in a specular direction, yielding a very low return to the SAR antenna. This phenomenon brings also a low interferometric coherence due to the consequent SNR decorrelation. Moreover, it is also known that a water body decorrelates within tens of milliseconds [31]. Although TanDEM-X is a bistatic mission built to avoid temporal decorrelations, the satellites formation brings small along-track time lags varying between 50 ms (equator) and 0 ms (poles). The global study performed in [32] demonstrated that from 10 ms water decorrelates. In the studied test case, the mean measured time lag of about 30 ms overcomes the limit. Several investigations have been proposed about the derivation of water bodies from the joint use of amplitude and coherence [32], [33]. In this paper the technique proposed by [32], operationally employed for the generation of water body mask as an auxiliary product of the official TanDEM-X DEM, is adopted. By analyzing 1700 randomly worldwide-distributed scenes, [32] established two thresholds that provided a correctness analysis well above 90 %. Specifically, a threshold value of 40 for the amplitude digital number (corresponding to -18 dB in radar brightness and about -20 dB in Sigma-Nought for the studied case) and 0.23 for the coherence were selected. Three water mask confidence levels are then generated: (1) detection from coherence threshold, (2) detection from amplitude threshold and (3) detection from both thresholds. The third level represents the highest confidence one. In this study, this strategy is applied for scenes having flooded crops. In Fig. 8, the 12.05.2012 amplitude and coherence data show the flooded parcels for that date with low values. As visible, not all the fields were already flooded (see also Fig. 2). To better cover the test site, additional information is retrieved by using also the 21.05.2013 and 01.06.2013 acquisitions.

A potential issue in the detection relies in the presence of wind during the acquisition. For the Rayleigh criterion, a surface is regarded as specular if its vertical variation is smaller than about 5 mm for X-band at 36.8 deg [30]. Wind may induce waves with height well above this value resulting in backscattered energy at the sensors. Thus, amplitude threshold can result too low for these cases and can generate misdetections. Nevertheless, water decorrelation yields low coherence and water results masked with the second confidence level [20]. In the study area, the highest confidence level is reached for all the detections indicating a proper threshold selection for both amplitude and coherence. Even though not representing the studied scenario, false detections can arise due to volume decorrelation on forested areas or on geometrical decorrelation zones (radar shadow/layover). While a DEM is helpful to discard detection on slopes (i.e. on mountain shadows), a false color composite (FCC) using coherence, backscatter and differential backscatter has been demonstrated useful to generate land cover maps to discard forest and urban settlements from the water mask [34].

Straight after the water detection, a binary morphological

erosion with a $3 - by - 3$ rectangular structuring element is performed to remove isolated artifacts and a binary shape fill is performed to remove possibly remaining holes within shapes. The final mask is then segmented and the fields numbered. A total of more than 2000 fields are detected. The detection and the segmentation are performed in the geocoded domain, in order to easily compare them with ground truth data. To be noticed, geolocation errors hardly occur due to the precise calibration and the practically flat scenario. In this test site, segmentation errors may manifest due to the path length between fields (3 to 8 meters). Considering the DEM spacing of 6 meters and the resolution of about 10 meters, paths span just 1-2 pixels, possibly creating false linking between regions. Nevertheless, the comparison between the segmentation and the ground truth for the 8 fields chosen for the analysis reveals a good matching with an average completeness of 91%, defined as the ratio between the segmented field and the reference one. The remaining 9% may be attributed to the erosion procedure with a square element.

Fig. 7 shows the mean 2012 coherence values for detected flooded fields on 12.05.2012 (red points) and the mean 2013 values for fields flooded on 21.05.2013 (green points). The 2012 acquisitions, spanning the plant growing cycle, exhibit the good quality of the derived elevation for all the stages (June-September) excluding the early vegetative stage (May). A coherence of around 0.2 for the May acquisition (flooded field) yields not reliable elevation values. Moreover, this value results overestimated due to the estimation bias caused by the finite estimation support of 11 by 11 samples [35]. Accurate heights are instead generated for the later data. Coherence fluctuates around 0.8 for the June-July data with a decreasing trend mainly caused by the increasing height of ambiguity for similar field conditions (wet environment, fresh plants). This value increases for the following two acquisitions (August-September) as the field condition switches to dense vegetation, ideally behaving like a distributed scatterer. To be noticed, a coherence value of around 0.85 corresponds to better height accuracy than the one specified in Tab. II. The last two 2012 acquisitions are over the plant cycle, after the harvesting. Here, coherence around 0.9 indicates very accurate elevation values, as the field condition transformed to bare soil with a very rough surface yielding high SNR. The last acquisition, November 2012, is taken as reference as indicates the terrain height without water or rice plants. The 2013 acquisition are also showed in Fig. 7 for completeness. The first two data cover the early-year period prior the plantation and have huge coherence variations, also denoting poor elevation accuracy. The field detection is performed for the late May acquisition, showing a similar value and accuracy to the one used for the 2012 field extraction. The prior and following data provide a higher coherence with high variations, indicating non-homogeneous conditions for the fields under analysis. The last two acquisitions, in the reproductive stage, follow the same trend of the 2012 one.

Fig. 9 visually shows the plant growth of July 06, August 19 and September 10, 2012. The differences with the reference height of November 2012 are here represented with an overlay between the amplitude and the mean height difference for all

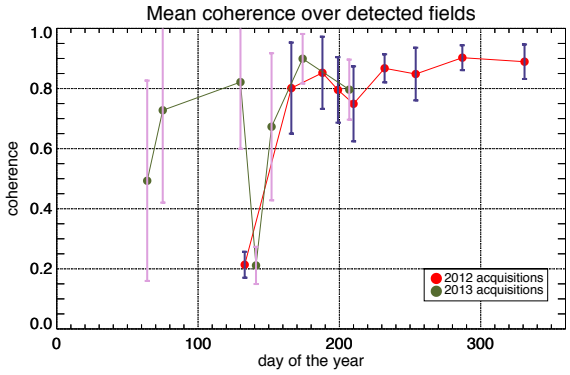

Fig. 7. Mean coherence trend for the fields extracted by using the 12.05.2012 acquisition (red line) and by using the 21.05.2013 acquisition (green line). The standard deviation is highlighted with error bars.

(a) amplitude

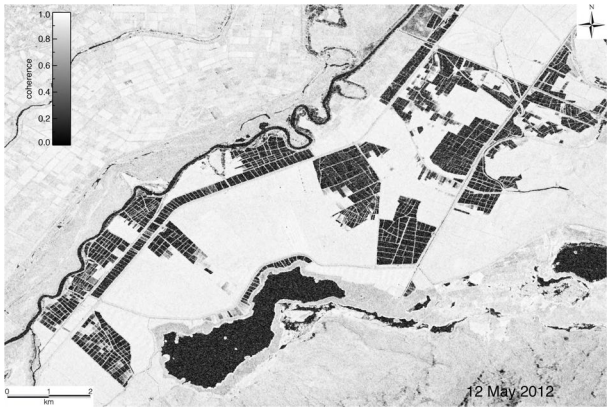

(b) coherence

Fig. 8. SAR master channel amplitude (left) and interferometric coherence (right) of the 12.05.2012 TanDEM-X acquisition, used to extract field shapes.

the detected fields having an average coherence above 0.8 for both the analyzed and the reference acquisitions. Inspecting these maps, one could check the growing trend on a field-by-field basis. For instance, the July map in Fig. 9(a) shows a quite homogeneous result with plant heights around 70 cm. The August map in Fig. 9(b) reveals the growing of most of the plants, with doubled heights compared to Fig. 9(a). For some of the fields, the higher maturation level is reached about a month later, as visible in Fig. 9(c). In general, these maps can

be used for the agricultural planning, in terms of production volume and outcomes.

Finally, to highlight the TanDEM-X capability in assessing the temporal crop growth, in Fig. 10 the mean height for the 2012 detected fields (flooded in Fig. 8) is shown in black and the standard deviation highlighted in purple. The reference temporal elevation is over-plotted. Although a detailed validation is provided in the next section, the mean trend already shows a good accordance with the reference. The height deviation for the late July acquisitions has to be linked to the different growing periods of the detected fields.

C. Relationship between canopy height and inteferometric phase

In this section the analysis and the validation of the derived elevation with respect to the field measurements is assessed. Fig. 10 already provides a visual overview of the reference elevation data and the mean TanDEM-X trends. Here, three out of eight fields (marked in Fig. 9(a)) are studied in detail with the analysis depicted in Fig. 11. The results from the other fields are not shown since they perform very similar to the selected three fields.

Before entering in the analysis of the current data set, it is meaningful to predict the expected height for the vegetation in the general electromagnetic framework. It is well known that the interferometric phase is proportional to the height of the scattering phase center. The phase center location depends on the complex interaction of the microwave signal with the imaged surface. For canopies, it is usually below the top of the vegetation as the transmitted signal travels within the medium, penetrating into it [36]. The degree of penetration is characterized by the extinction coefficient, a parameter depending on the system wavelength and the effective dielectric constant of the imaged medium. In particular, extinction coefficient is inversely proportional to the wavelength and directly proportional to the imaginary part of the effective dielectric constant. This corresponds to an increased penetration depth for large wavelengths and for reduced moisture content in the medium. Considering the interferometric analysis, the smaller the extinction, the lower the scattering center. Consequently, the retrieved elevation will be equal or smaller depending on the actual effective dielectric constant of the canopy (and the ground), since in the proposed approach the canopy height is retrieved with a difference between a plant growing phase and bare soil - the latter from a post-harvest data take. In the following, the interpretation based on the current experiment is provided.

An important remark for the comparison between interferometric heights and ground truth data relies on the different years of the two data source. As beforehand underlined, the sole 2012 TanDEM-X data full covers the growing stages and is used for validation despite the campaign has been performed in 2013. In practice, validation inaccuracies could take place depending on the seeding date decided by the field owner. For the fields under analysis the seeding date discrepancy between the two years has been stated to be less than a week, thus strongly limiting this error source. A second inaccuracy source

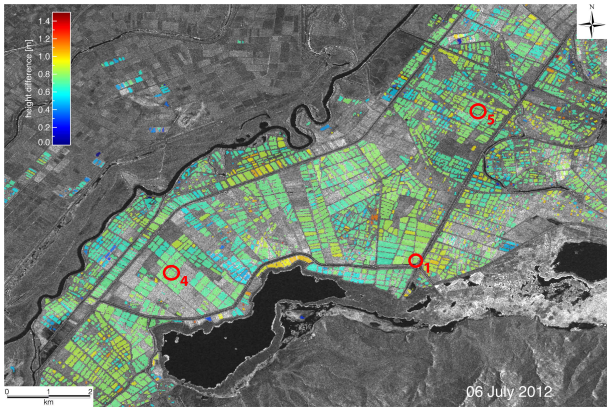

(a) 06.07.2012

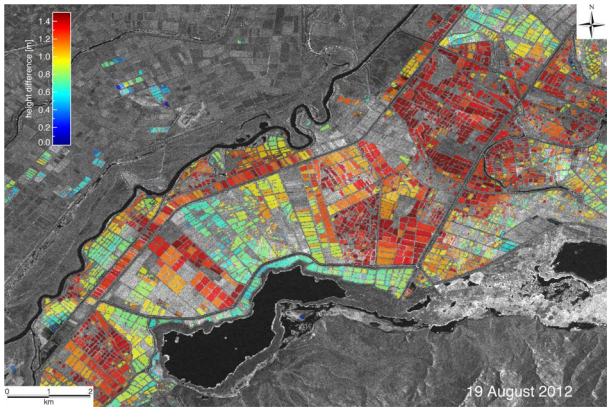

(b) 19.08.2012

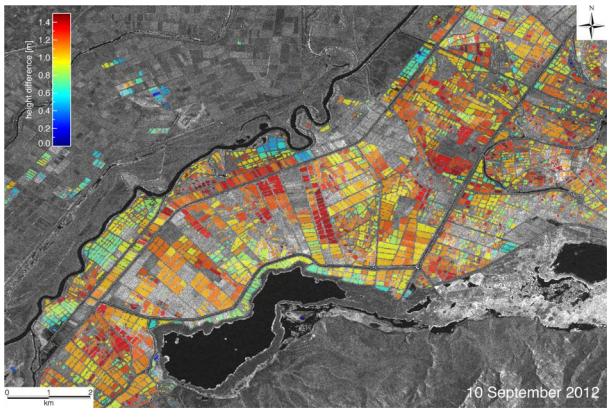

(c) 10.09.2012

Fig. 9. Temporal 2012 height change analysis. The difference between the (06.07, 19.08, 10.09) acquisitions and the reference one in 26.11 is shown in the subfigures (a), (b) and (c) respectively. The changes are shown in a field by field basis, for fields having coherence higher than 0.8 for both the analyzed and reference acquisitions. The three fields under analysis in Section III-C are marked in (a).

resides in changes in plant moisture variations between the two years, manifesting in a root mean square error increase due to the different penetration into the canopy.

The differential-InSAR-based and the field-measurement-based canopy height is shown in Fig. 11 along with the BBCH-scale measurement as reference. The 6 TanDEM-X measurements (June to September 2012) are not well spanned as the 11 ground measurements (June to September 2013)

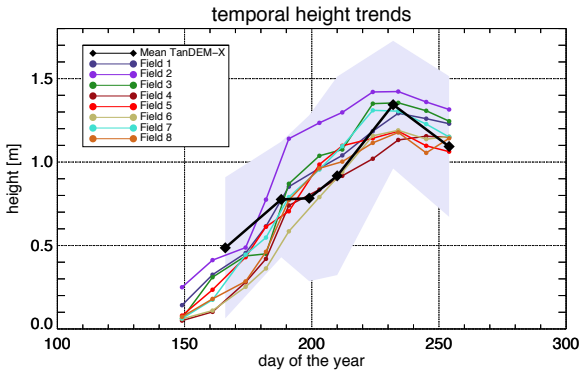

Fig. 10. Mean temporal TanDEM-X elevation trend for 2012 detected fields (black) and corresponding standard deviation (purple). The reference fields are overplotted with colors in the legend.

but show common peculiarities. As already reported in the previous section, the elevation trend is well detected by the interferometric measure for the late vegetative phase, reproductive and maturation stages. Instead, the early vegetative phase represented by the May 2012 acquisition yields strongly biased elevation values and is not considered in the following analysis.

The June acquisition corresponds to the central vegetative stage (tillering, Tab. I). At this phase, plants emerge from water (see the second and the third picture in the second row in Fig. 2). In the SAR resolution cell different phenomena as double scattering, water reflection and surface reflections combine together. The interferometric elevation results underestimated, showing a mean difference with reference data of 7.7 cm for all the 8 fields under study. A singular exception is measured for the field 5 in Fig. 11(c), with an overestimation of about 10 cm, to be attributed to a lower coherence value and a higher phase noise. For this take, double bounces between growing vegetation and standing water should be the dominant part of the radar return. The aforementioned scattering phase center is located at the water elevation for the cardinal effect on corners - in this case represented by quasi-vertical stems on calm water. However, the small measured height difference suggests the partial presence of the phenomenon due to the use of a short wavelength (3.1 cm) at a relatively high incidence angle (about 37 deg) yielding a limited penetration of the echo inside the fresh vegetated volume. For the three July measurements the elevation is largely underestimated, with a mean difference of 26.5 cm. Also this discrepancy, in the end of the vegetative stage and beginning of the reproduction (booting-heading, Tab. I), can be explained with the radar wave interaction with the inner part of fresh canopy (see fourth picture in the second row in Fig. 2). The August acquisition exhibits instead a generally good matching, with a mean underestimation of 4.8 cm. Being at the beginning of the maturation stage (fifth picture in the second row in Fig. 2), plants start to densely produce milky grains at their surface which reflect the signal at X-band. The last considered acquisition, in September, falls at the end of the maturation (seventh picture in the second row in Fig. 2). The grain is dry and mature, with a maximum height slightly smaller than the previous stage. On this date

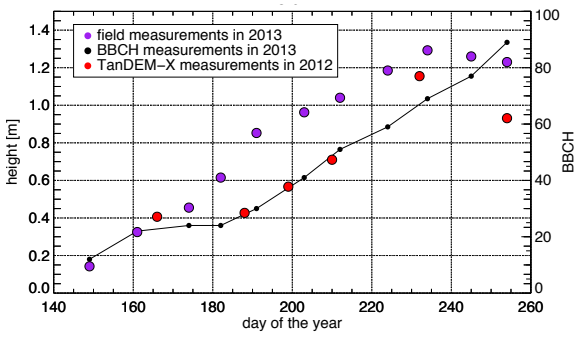

(a) field1

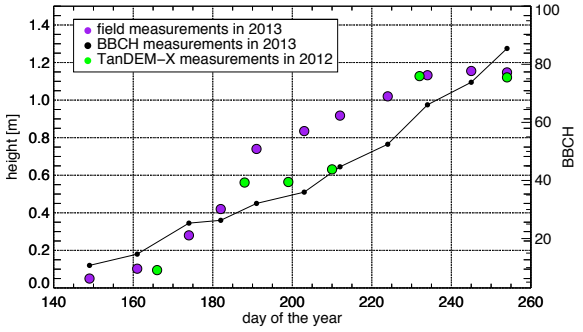

(b) field4

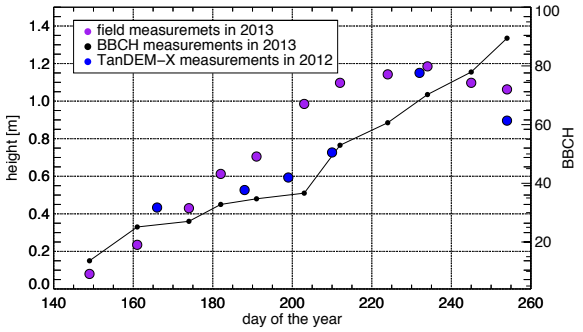

(c) field5

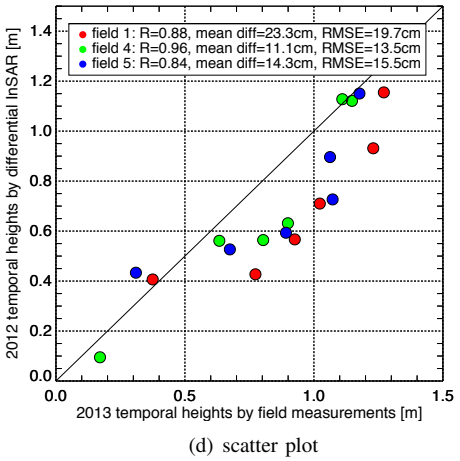

(d) scatter plot

Fig. 11. Comparison of height measurements, superimposed over temporal BBCH scales, between the ground measurements (purple circles) held in 2013 and the one from bistatic interferometry ((a) red, (b) green, (d) blue circles) in 2012 over the 3 different fields shown in Fig. 9(a). (d) the corresponding scatter plot with quantitative analysis at the top.

the interferometric elevations result again underestimated on average, with a mean difference of 16 cm. In principle, at this stage, plant elements are more randomly oriented and drier than in previous ones, hence making more similar the propagation for all polarizations. Nevertheless, an higher phase center is measured for the VV polarization as shown in Fig. 5(c). The reason relies in the lower backscattering component from the volume, due to its drier condition, hence increasing the relative importance of the double-bounce contribution to the backscattered signal, which is located at the ground surface. Since the double-bounce contributes more to HH than to VV, the phase center is more close to the ground at HH than at VV, and hence the higher phases at VV than at HH. Following this consideration, a more accurate elevation result can be generated using VV channel.

For completeness, a best fit analysis in the form of $y = ax + b$ is used for calculating the offset between the two measurements. The corresponding scatter plot is in Fig. 11(d). Due to the growing height trend in time, this plot can be easily interpreted in a similar way of the others in Fig. 11. The generally underestimated InSAR tendency is more noticeable in the center portion of the plot, for the reproductive stage. As the data time sampling is not overlapping, a linear interpolation for the reference at the InSAR locations is performed, with possible errors coming from the non-linearity of the plant growth attenuated by the fine reference sampling (see Fig. 11(a) - 11(c)). The two sources result highly correlated, with a correlation coefficient R equal to 0.88, 0.96 and 0.84 for the three fields under analysis. The mean differences and root mean square errors are in the decimetric level. In detail, the mean differences between reference and InSAR result 23.3, 11.1 and 14.3 cm and the root mean square error 19.7, 13.5 and 15.5 cm. Even though the scattering analysis and the quantitative evaluation performed on this section are useful to understand the overall process, the focus shall be on the centimeter accuracy of the system for this application, and its capability of temporarily tracking the elevation through most of all the growing stages of paddy rice fields.

IV. Conclusions

The outcomes presented in this paper underline that X-band differential bistatic interferometry, which is of great benefit in observing surface height changes, has a great potential in paddy rice elevation mapping and can provide input to production estimation in terms of volumetric changes. A test site widely employed for rice production in Turkey has been investigated with 16 dual-pol TanDEM-X acquisitions spanning two years and a dedicated ground campaign. The research demonstrates that for absolute ranging studies at X-band wave polarization is not particularly relevant - only small elevation discrepancies around 8 cm were measured in dry season. Nevertheless, polarization is of fundamental importance for every other study on physical parameters. For instance, the HH/VV backscatter ratio, an instrument to classify the different phenological stages is presented in the paper as well. The Integrated TanDEM-X Processor is employed for raw DEM generation and internal calibration with freely available references as SRTM and ICESat. Fields are then individually extracted in the interferometric processor without external references by searching for flooded areas during the rice early vegetative stages. This segmentation allows the elevation tracking on a field-by-field basis, being attractive for separated crop inspections. The absolute approach is then made differential with the objective of volumetric production assessment. Height differences with a digital terrain model, derived in this case from the dataset itself employing a post-harvest data take, yield the direct validation with ground truth measurements. The increasing temporal elevation trend is well derived by TanDEM-X, with a general underestimation especially in the reproductive rice stage due to the wave interaction with lower portions of the plant. The root mean square error is contained between few centimeters and about 20 cm, depending on the actual phenological phase. Although plant elevations are tracked with a good accuracy for most of the plant growing phases, the main limitation relies on the inability to map plant heights at early growing stages due to the lack of coherence in the data. In conclusion, as already seen in other geophysical domains, this specific application strengthens the use of bistatic SAR interferometry for the tracking of dynamical earth elevation changes.

Acknowledgments

Authors would like to acknowledge the anonymous reviewers for their helpful contributions to improve the overall paper quality as well as the colleagues A. Parizzi and I. Hajnsek for the fruitful scientific discussions on the paper topics and H. Breit, T. Fritz and F. Rodriguez-Gonzalez for the processing supervision in handling experimental data in an operational and systematic way. The *Rice and Wetlands monitoring in Turkey* project is performed by funding of The Scientific and Technological Research Counsil of Turkey (TUBITAK project no: 113Y446). TanDEM-X SAR data were supplied by German Aerospace Center under the project no: XTILAND1476.

References

[1] P. Lancashire, H. Bleiholder, T. Boom, P. Langelüddeke, R. Stauss, E. Weber, and A. Witzenberger, "A uniform decimal code for growth stages of crops and weeds," *Annals of Applied Biology*, vol. 119, no. 3, pp. 561–601, 1991.

[2] S. Yun, F. Xiangtao, L. Hao, X. Jianhua, S. Ross, B. Brisco, R. Brown, and G. Staples, "Rice monitoring and production estimation using multitemporal RADARSAT," *Remote Sensing of Environment*, vol. 76, no. 3, pp. 310–325, 2001.

[3] M. Chakraborty, K. R. Manjunath, S. Panigrahy, N. Kundu, and J. S. Parihar, "Rice crop parameter retrieval using multi-temporal, multi-incidence angle RADARSAT SAR data," *ISPRS Journal of Photogrammetry and Remote Sensing*, vol. 59, pp. 310–322, 2005.

[4] P. Patel, H. S. Srivastava, S. Panigrahy, and J. S. Parihar, "Comparative evaluation of the sensitivity of multi-polarized multi-frequency SAR backscatter to plant density," *International Journal of Remote Sensing*, vol. 27, no. 2, pp. 293–305, 2006.

[5] C. Wang, J. Wu, Y. Zhang, G. Pan, J. Qi, and W. A. Salas, "Characterizing L-band scattering of paddy rice in southeast China with radiative transfer model and multitemporal ALOS/PALSAR imagery," *Geoscience and Remote Sensing, IEEE Trans. on*, vol. 47, pp. 988–998, 2009.

[6] A. Bouvet, T. Le Toan, and N. Lam-Dao, "Monitoring of the rice cropping system in the Mekong delta using ENVISAT/ASAR dual polarization data," *Geoscience and Remote Sensing, IEEE Trans. on*, vol. 47, pp. 517–526, 2009.

[7] E. Erten, A. Reigber, L. Ferro-Famil, and O. Hellwich, "A new coherent similarity measure for temporal multi-channel scene characterization," *Geoscience and Remote Sensing, IEEE Trans. on*, vol. 50, no. 7, 2011.

[8] H. S. Srivastava, P. Patel, Y. Sharma, and R. R. Navalgund, "Multi-frequency and multi-polarized SAR response to thin vegetation and scattered trees," *Current Science*, vol. 97, no. 3, pp. 425–429, 2009.

[9] I. Choudhury, M. Chakraborty, S. C. Santra, and J. S. Parihar, "Methodology to classify rice cultural types based on water regimes using multitemporal RADARSAT-1 data," *International Journal of Remote Sensing*, vol. 33, pp. 4135–4160, 2012.

[10] Y. Inoue, E. Sakaiya, and C. Wang, "Capability of C-band backscattering coefficients from high-resolution satellite SAR sensors to assess biophysical variables in paddy rice," *Remote Sensing of Environment*, vol. 140, pp. 257–266, 2014.

[11] S. L. Durden, L. A. Morrissey, and G. P. Livingston, "Microwave backscatter and attenuation dependence on leaf area index for flooded rice fields," *Geoscience and Remote Sensing, IEEE Trans. on*, vol. 33, no. 3, pp. 807–810, 1995.

[12] J. M. Lopez-Sanchez, J. D. Ballester-Berman, V. D. Navarro-Sanchez, and F. Vicente-Guijalba, "Experimental validation of the interferometric coherence formulation in single-transmit mode," in *Geoscience and Remote Sensing Symposium, 2012. IGARSS 2012. IEEE International*, 2012, pp. 3114–3117.

[13] J. M. Lopez-Sanchez and J. D. Ballester-Berman, "Potentials of polarimetric SAR interferometry for agriculture monitoring," *Radio Science*, vol. 44, no. 2, 2009.

[14] J. M. Lopez-Sanchez, J. D. Ballester-Berman, and I. Hajnsek, "First results of rice monitoring practices in Spain by means of time series of TerraSAR-X dual-pol images," *IEEE Journal of Selected Topics in Applied Earth Observations and Remote Sensing*, vol. 4, pp. 412–422, 2011.

[15] J. M. Lopez-Sanchez, I. Hajnsek, and J. D. Ballester-Berman, "First demonstration of agriculture height retrieval with PolInSAR airborne data," *Geoscience and Remote Sensing Letters, IEEE*, vol. 9, no. 2, pp. 242–246, 2012.

[16] J. M. Lopez-Sanchez, F. Vicente-Guijalba, J. D. Ballester-Berman, and S. R. Cloude, "Polarimetric response of rice fields at C-band: Analysis and phenology retrieval," *Geoscience and Remote Sensing, IEEE Trans. on*, vol. 52, no. 5, pp. 2977–2993, 2013.

[17] J. M. Lopez-Sanchez, S. R. Cloude, and J. D. Ballester-Berman, "Rice phenology monitoring by means of SAR polarimetry at X-band," *Geoscience and Remote Sensing, IEEE Trans. on*, vol. 50, no. 7, pp. 2695–2709, 2012.

[18] U. Wegmüller and C. Werner, "Retrieval of vegetation parameters with SAR interferometry," *Geoscience and Remote Sensing, IEEE Trans. on*, vol. 35, no. 1, pp. 18–24, 1997.

[19] M. E. Engdahl, M. Borgeaud, and M. Rast, "The use of ERS 1/2 tandem interferometric coherence in the estimation of agricultural crop heights," *Geoscience and Remote Sensing, IEEE Trans. on*, vol. 39, no. 8, pp. 1799–1806, 2001.

[20] H. S. Srivastava, P. Patel, and R. R. Navalgund, "Application potentials of synthetic aperture radar interferometry for land-cover mapping and crop-height estimation," *Current science*, vol. 91, no. 6, pp. 783–788, 2006.

[21] F. De Zan, A. Parizzi, P. Prats-Iraola, and P. López-Dekker, "A SAR interferometric model for soil moisture," *Geoscience and Remote Sensing, IEEE Trans. on*, vol. 52, no. 1, pp. 418–425, 2014.

[22] E. Erten, "Glacier velocity estimation by means of a polarimetric similarity measure," *Geoscience and Remote Sensing, IEEE Trans. on*, vol. 51, no. 6, pp. 3319–3327, 2013.

[23] E. Erten, A. Reigber, and O. Hellwich, "Generation of three-dimensional deformation maps from InSAR data using spectral diversity techniques," *ISPRS Journal of Photogrammetry and Remote Sensing*, vol. 65, no. 4, pp. 388–394, 2010.

[24] C. Rossi and S. Gernhardt, "Urban DEM generation, analysis and enhancements using TanDEM-X," *ISPRS Journal of Photogrammetry and Remote Sensing*, vol. 85, pp. 120–131, 2013.

[25] G. Krieger, A. Moreira, H. Fiedler, I. Hajnsek, M. Werner, M. Younis, and M. Zink, "TanDEM-X: A satellite formation for high-resolution SAR interferometry," *Geoscience and Remote Sensing, IEEE Trans. on*, vol. 45, no. 11, pp. 3317–3341, 2007.

[26] J. M. Lopez-Sanchez, F. Vicente-Guijalba, and J. D. Ballester-Berman, "The problem of SNR in PolInSAR observations with TanDEM-X over rice fields." in *4. TanDEM-X Science Meeting, 12-14 June 2013, DLR Oberpfaffenhofen*, 2013.

[27] D. Just and R. Bamler, "Phase statistics of interferograms with applications to synthetic aperture radar," *Applied optics*, vol. 33, no. 20, pp. 4361–4368, 1994.

[28] C. Rossi, F. R. Gonzales, T. Fritz, N. Yague-Martinez, and M. Eineder, "TanDEM-X calibrated raw DEM generation," *ISPRS Journal of Photogrammetry and Remote Sensing*, vol. 73, pp. 12–20, 2012.

[29] H. Breit, T. Fritz, U. Balss, M. Lachaise, A. Niedermeier, and M. Vonavka, "TerraSAR-X SAR processing and products," *Geoscience and Remote Sensing, IEEE Trans. on*, vol. 48, no. 2, pp. 727–740, 2010.

[30] F. M. Henderson and A. J. Lewis, *Principles and applications in imaging radar*. New York:Wiley, 1998.

[31] R. Bamler and P. Hartl, "Synthetic aperture radar interferometry," *Inverse problems*, vol. 14, no. 4, 1998.

[32] A. Wendleder, B. Wessel, A. Roth, M. Breunig, K. Martin, and S. Wagenbrenner, "TanDEM-X water indication mask: Generation and first evaluation results," *International Journal of Applied Earth Observation and Geoinformation*, vol. 6, no. 1, pp. 171–179, 2013.

[33] G. Nico, M. Pappalepore, G. Pasquariello, A. Refice, and S. Samarelli, "Comparison of SAR amplitude vs. coherence flood detection methods-a GIS application," *International Journal of Remote Sensing*, vol. 21, no. 8, pp. 1619–1631, 2000.

[34] H. S. Srivastava, P. Patel, S. N. Prasad, Y. Sharma, B. A. Khan, B. Praveen, K. C. A. Prasad, S. Sharma, L. Vijayan, and V. S. Vijayan, "Potential applications of multi-parameteric Synthetic Aperture Radar (SAR) data in wetland inventory: A case study of Keoladeo National Park (A world heritage and Ramsar site), Bharatpur, India." in *in Proc. Taal 2007: The 12th World Lake Conference*, 2008, pp. 1862–1879.

[35] R. Touzi, A. Lopes, J. Bruniquel, and P. W. Vachon, "Coherence estimation for SAR imagery," *Geoscience and Remote Sensing, IEEE Trans. on*, vol. 37, no. 1, pp. 135–149, 1999.

[36] K. Sarabandi and Y. C. Lin, "Simulation of interferometric SAR response for characterizing the scattering phase center statistics of forest canopies," *Geoscience and Remote Sensing, IEEE Trans. on*, vol. 38, no. 1, pp. 115–125, 2000.

Cristian Rossi received the Laurea Magistrale (M.Sc.) degree in telecommunication engineering from Politecnico di Milano, Milan, Italy, in 2006. From 2006 to 2008, he was project engineer with Aresys s.r.l. -a Politecnico di Milano spin-off company-. Since 2008, he is with the SAR Signal Processing Department, Earth Observation Center, German Aerospace Center (DLR), Oberpfaffenhofen, Germany, where he works on the development of the Integrated TanDEM-X Processor (ITP) and on novel interferometry algorithms for SAR missions. His research interests focus on urban remote sensing, multi-source data fusion, digital elevation models, and Doppler shift estimation for ocean currents.

Esra Erten received the B.S degree in Geodesy and Photogrammetry Engineering and the M.S.E.E. degree in Satellite Communication and Remote Sensing from Istanbul Technical University (ITU), Turkey, in 2003 and 2005, respectively. She took the Ph.D. degree from the department of Computer Vision and Remote Sensing at Berlin University of Technology, 2010. She was with the High-Frequency Institute, German Aerospace Center (DLR), Oberpfaffenhofen, Germany, from April 2008 to June 2010, where she worked on information theory for multi-channel SAR images. From 2010 to 2012, she was with the Chair of Earth Observation and Remote Sensing, Institute of Environmental Engineering, ETH Zurich, where she worked on applied radar remote sensing for environmental parameter estimation. Currently, she is an associated professor at the department of Geomatics Engineering, Faculty of Civil Engineering, ITU, Istanbul. Her research interests include information extraction and image understanding from SAR and optical images; in particular information theory, multivariate statistics, polarimetry, interferometry, and hyper-spectral imaging.